Pergamon

J. Aerosol Sci. Vol. 30, No. 3, pp. 325–340, 1999

Printed in Great Britain
0021-8502/99 $19.00 + 0.00

PII: S0021-8502(98)00064-0

AN EXPERIMENTAL STUDY ON THE PERFORMANCE OF A SINGLE DISCHARGE WIRE-PLATE ELECTROSTATIC PRECIPITATOR WITH BACK CORONA

Chung-Liang Chang and Hsunling Bai*

Institute of Environmental Engineering, National Chiao Tung University, 75, Po-Ai St., Hsin-Chu, 30039, Taiwan

(*First received* 3 *November* 1997; *and in final form* 21 *April* 1998)

Abstract—The phenomenon of back corona is well known in that it may reduce the collection efficiency of an electrostatic precipitator. In this study, experimental results are presented for the influence of back corona on the performance of a laboratory scale single-discharge-wire ESP system. The effect of back corona under two power controlled methods, constant voltage operation and constant current operation, has been evaluated. The experimental results showed that as back corona occurs, the output current and the power consumption are increased under constant voltage operation. The mass collection efficiency is proportional to the applied voltage. On the other hand, for constant current operation the voltage and the power consumption are decreased under back corona. The mass collection efficiency is independent of the applied current. A lateral mixing model was also applied to assist in the discussion of corona power and particle collection efficiency under normal and stable back corona conditions. Both experimental and theoretical results indicated that the back corona has a large effect on submicron particles. The grade efficiency can be reduced by over 60% for submicron particles. The large reduction of efficiency for submicron particles is due to significant reduction in both particle charge and migration velocity. Since particles in the submicron region are more sensitive to light scattering, the opacity problem may be aggravated under back corona.

NOMENCLATURE

A_c	collection plate area, m^2
b^-	electric mobility of negative ions, $m^2\,V^{-1}\,s^{-1}$
b^+	electric mobility of positive ions, $m^2\,V^{-1}\,s^{-1}$
C	Cunningham slip correction factor, dimensionless
C_D	drag coefficient, dimensionless
d_p	particle diameter, m
E	local electric field, $V\,m^{-1}$
E_{av}	average field strength, $V\,m^{-1}$
E_c	electric field strength at the surface of the corona wire, $V\,m^{-1}$
E_i	the electric field strength at the boundary of the ionized sheath, $V\,m^{-1}$
E_p	collecting field strength on the collection plate, $V\,m^{-1}$
I_i	corona current on the corona wire, A
J	current density, $A\,m^{-2}$
J_p	current density on the collection plate, $A\,m^{-2}$
k	Boltzmann constant, $J\,K^{-1}$; 1.38×10^{-23}
L	length of the collection plate, m
L_w	length of discharge wire, m
m_p	mass of a particle, kg
Q	volumetric flow rate of gas through an ESP, $m^3\,s^{-1}$
q	charge on the particle, C
q_e	electronic unit charge, C; 1.6×10^{-19}
r_i	the radius of the ionized sheath, m
S	degree of back corona, see equation (A10), dimensionless
T	stream temperature, K
t	residence time, s
u_F	gas flow velocity, $m\,s^{-1}$
u_p	particle velocity, $m\,s^{-1}$
V	local voltage, V
V_a	applied voltage, V
W	plate-to-plate space, m

*Author to whom correspondence should be addressed.

Greek letters

ε_o permittivity in a free space, $F\,m^{-1}$; 8.85×10^{-12}
η collection efficiency, dimensionless
μ fluid viscosity, $m^2\,s^{-1}$
ρ_i the corona space-charge density of the wire, $C\,m^{-3}$
ρ_- negative space charge density, $C\,m^{-3}$
ρ_+ positive space charge density, $C\,m^{-3}$
ρ_{-s} negative space charge density on the surface of collection plates, $C\,m^{-3}$
ρ_{+s} positive space charge density on the surface of collection plates, $C\,m^{-3}$
ρ_p particle density, $kg\,m^{-3}$
ρ_F air density, $kg\,m^{-3}$
ω effective migration velocity of a particle, $m\,s^{-1}$

Subscript

i ith particle size
j jth position

INTRODUCTION

The electrostatic precipitator (ESP) is one of the most commonly applied particulate control devices to reduce fly-ash emission from utility boilers, incinerators and many industrial processes. The corona power of the ESPs directly governs the collection efficiency of the system. The collection efficiency is increased as corona power increases. The increase of corona power refers to the increase of voltage or current applying to the system. However, when high resistivity dust particles deposit on the surface of collecting plates, the ideal design of an ESP is changed. One of the major problems for a wire discharge system is back corona. The performance of a discharge system, either the commercial wire-plate ESP or the single discharge wire system for a two-stage ESP, is damaged by back corona (Kwetkus, 1997).

Both experimental work and plant experience indicated that back corona can in some cases begin to form at layer resistivities around 2×10^8 ohmmeters, and their intensity rises alarmingly from some $10^9\ \Omega$m onwards (White, 1974; Bohm, 1982; McLean, 1988). The physical phenomena of a back corona are always the same: a lower spark-over voltage, a higher current flow, and a loss of collecting efficiency. The particle layer on the collection plate breaks down electrically, which produces small craters and visible back corona discharges occur. A back corona reduces the spark-over voltage, and thereby narrows the voltage interval within which the unit can be operated. The formation of the positive-ion current leads to a rapid increase in the slope of the voltage–current characteristic. This is due to the increased number of positive and negative ions and can be large so as to give near-vertical or even negative slopes to the V–I curves (Lawless and Sparks, 1980). Besides, positive ions will flow back into the gas stream which are attracted by the existing negatively charged particles. Under back corona conditions the particle path changes substantially, they are apt to move reversely and often oscillate back and forth in an irregular fashion (Bohm, 1982).

Patel *et al.* (1985) experimentally reported the influence of back corona on the performance of a wire-plate precipitator. Their results showed that under constant applied electric field, the effective migration velocity decreased rapidly with time, accompanied by a rapid increase of the current density. Masuda and Nonogaki (1986) experimentally studied the ratio of negative ions to positive ions in the back corona field of an ESP. They noted that the ratio rose with increasing total current density in the streamer-mode back discharging, but it remained almost to be a constant in the glow-mode back discharging. Turner *et al.* (1988) also pointed out that the effective migration velocity under the back corona condition would be reduced to about 20–30% of the normal condition.

Hoburg (1982) developed a quantitative model for the description of charge density and electric field structures in a cylindrical precipitator with back ionization. Lawless and Sparks (1980) developed a mathematical model to simulate the voltage–current characteristic and current density distribution in the duct of a wire-plate ESP. They have proposed various mechanisms of back corona generated on the surface of collecting plates. However, experimental measurements were not available to confirm their theory.

It seems that studies on the performance of a wire-plate ESP or a single wire discharge system under normal conditions can be easily found in the literature. However, complete

studies of ESP performance under back corona are limited. Besides, the effect of back corona on particles of different sizes has also not been reported. The objective of this study is to experimentally investigate the influence of back corona on the performance of a laboratory-scale single discharge wire-plate precipitator. The electric state and the ESP collection efficiency under normal and back corona conditions are compared and discussed with the assistance of a simple lateral mixing model.

EXPERIMENTAL SETUP

A schematic diagram of the experimental setup in this study is shown in Fig. 1. The carrier gas was generated by an air compressor. Moisture and air pollutants in the inlet gas stream were removed by passing the gas stream through an air dryer and a HEPA filter. The ESP was a single discharge wire-plate system (with dimensions of $W \times L \times H$: $12 \times 30 \times 7.6$ cm). The operation temperature was maintained at 130°C by preheat oven and heat tapes. A dust feeder (WDF-II, BGI) with a flow rate of 30 l min^{-1} was used to inject particles into the air stream. The ash loadings were in the range of 0.5–1.2 g m^{-3}. The total flow rate in the ESP was 109 l min^{-1}. The average residence time in the discharge system was 1.5 s. The mass concentration and size distribution of the particles before and after the precipitator were measured by a filter holder or a cascade impactor (Anderson 220).

Sampling ports were placed at the entrance and exit of the ESP where the duct i.d. was 1 in. To ensure isokinetic sampling, the sampling point was at the duct center and inline with the flow. And the sampling velocity was kept the same as the duct flow velocity of 3.6 m s^{-1}. Sampling biases for charged particles may be significant for the plastic tube (Vincent, 1989). But in this study the sampling probe, filter holder as well as the cascade impactor were made of stainless steel. Besides, the whole ESP system (including sampling devices) was grounded to minimize the loss of particles due to the electrostatic attraction force. Hence sampling biases due to charged particles were minimal. This was observed by that particles deposited on the probe walls were much less than those being collected.

The Arizona Silica particles (Sample ID.: SAE FIN A.T.D., ISO FINE T.D.) were used in this study to simulate particle behaviors in an ESP. The particle density was 2.3 g cm^{-3}. Particles larger than 38 μm were removed by a screening mesh (U.S.A. Standard testing sieve, No. 400) to avoid settling of particles in the ESP. Figure 2 shows the size distribution of dust particles used in the experiment. For the purpose of introducing back corona discharge, higher resistivity particles were prepared by keeping them in an oven at 250°C for 24 h to remove moisture and volatile materials. And for tests on normal operation of the ESP, the moisture content of the gas stream was increased by a water syringe pump to

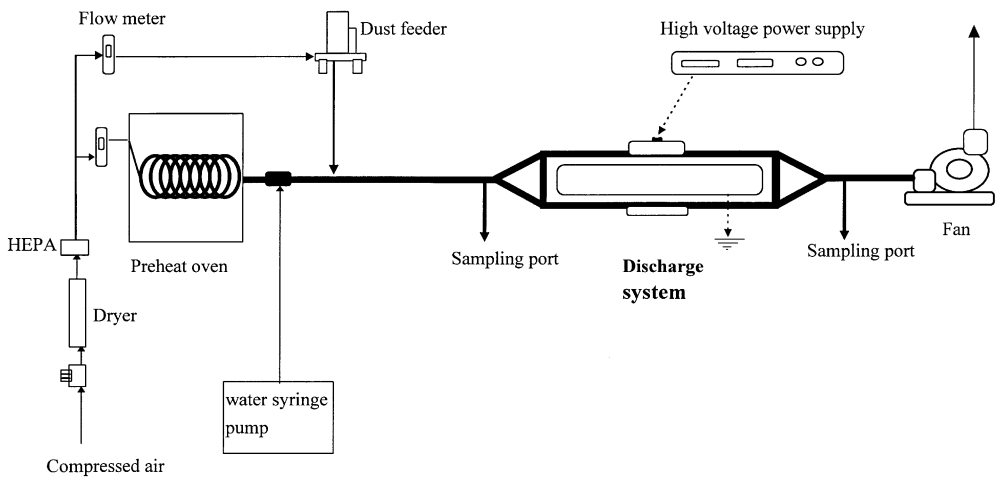

Fig. 1. Schematic diagram of the experimental setup.

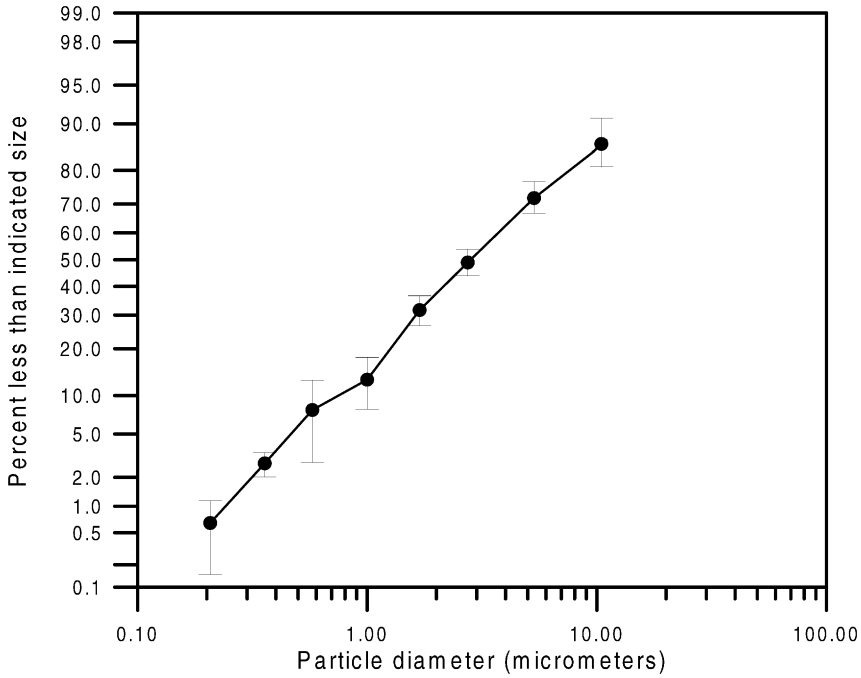

Fig. 2. The particle size distribution of standard dust particles.

reduce the particle resistivity. The moisture content of the gas under a normal condition was 6% (v/v).

The wire-plate precipitator was energized by a high-voltage DC supply (SPELLMAN, SL300) to generate a negative corona. Values of the output voltage and current were read directly from the power supply. Only one discharge electrode (diameter: 0.5 mm) was employed and located at the center of the ESP. There were two glass windows at the top of the discharge system for observing the phenomena occurring in the ESP.

RESULTS AND DISCUSSION

Constant applied voltage

Figure 3a shows experimental results on the variation of output current with operation time under a constant applied voltage. The collecting plates were cleaned before each test. Dusts of different resistivities were obtained with or without moisture conditioning. For the situation of without moisture conditioning, particles were inherent in a high resistivity problem and back corona condition of the ESP occurred. It is seen from Fig. 3a that there was a significant difference in output current between conditioning and without conditioning tests. As the system was conditioned by moisture injection, there was no obvious variation in the system power during the experimental test, and the output currents were around 0.2 ± 0.02 mA. But for the case of without moisture conditioning, the output currents seemed to significantly vary during the test period. The output currents increased in 10 min from around 0.18 to 1.2 mA and 1.4 mA, respectively, at applied voltages of 27 and 30 kV. The corona glow on the collecting plates was also observed for the case of without conditioning. These phenomena are the characteristics of back corona as described in the literature (White, 1974). The degree of oscillation of output current was large in the later period of the test. This is due to many unstable small break downs occurring in the dust layer. Comparing the difference between the applied voltages of 27 and 30 kV, one can see that the output current for the 30 kV applied voltage increased to higher values under

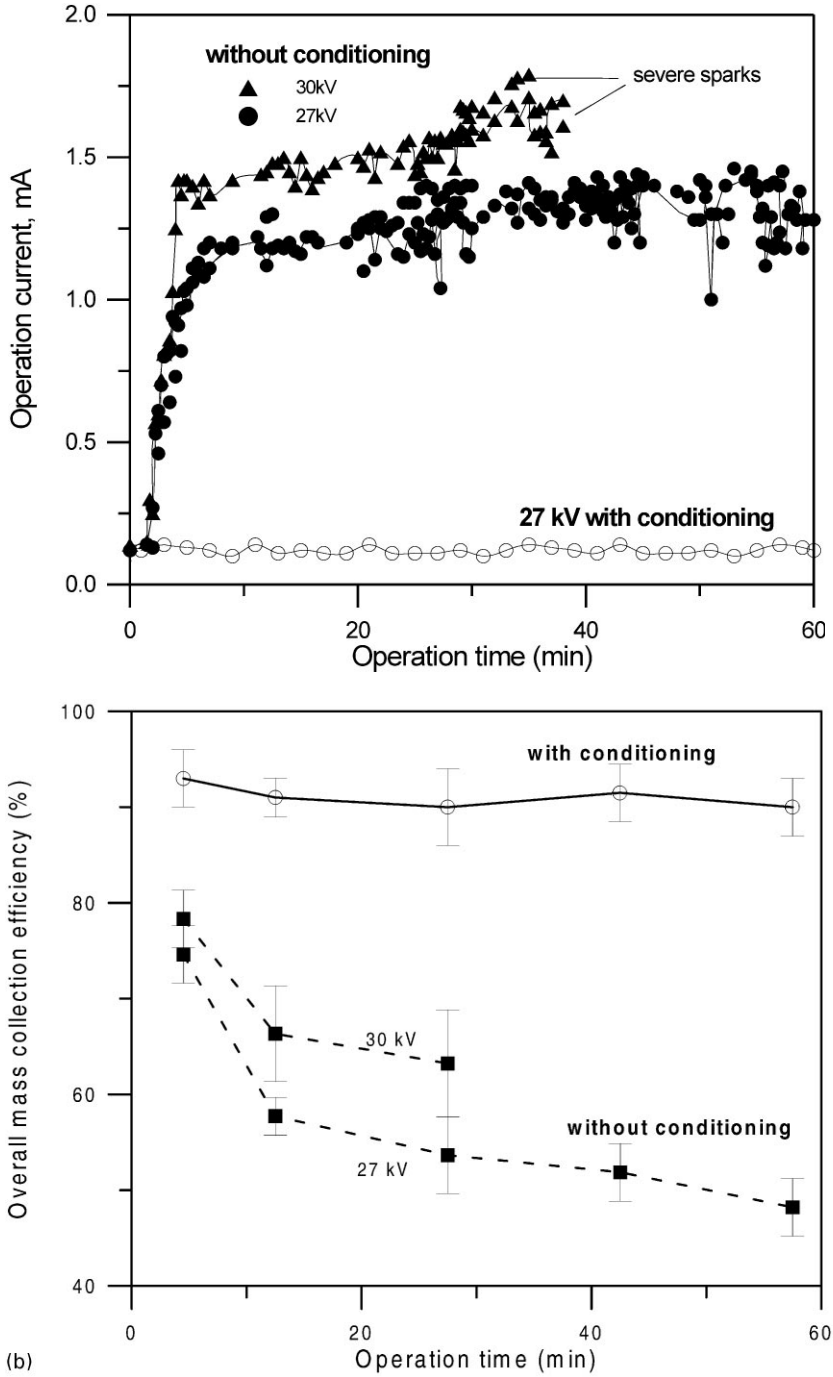

Fig. 3. Experimental results on the variation of (a) ESP output current with operation time under the constant applied voltage method and (b) overall mass collection efficiency with operation time under the constant applied voltage method.

the same operation time as that for 27 kV. And the test was stopped after 35 min of operation for the applied voltage of 30 kV due to the occurrence of severe sparks. For the applied voltage of 27 kV severe sparks were observed after 65 min of operation time.

Visible differences of dust layers deposited on the collecting plates between conditioning and without conditioning cases were also observed. For moisture conditioning test the dust layer was compact and smooth. But for the case of without conditioning, the dust layer was

very porous due to small break downs. As the spark was very severe, large craters were observed on the plate.

Experimental results of overall mass efficiency under normal and back corona conditions are shown in Fig. 3b as a function of operation time. When moisture conditioning was employed, the overall mass efficiencies had no obvious variation with time. The overall mass efficiencies were kept stable at around 90%. But for the case of without conditioning, the collection efficiencies dropped significantly during the test period. It is also observed by comparing Figs 3a and b that the rate of change of mass efficiency was related to the output current. The collection efficiency decreased with an increase of power consumption. After around 10 min, the variation of current and mass efficiency reached stable values for the case of without conditioning. It seems that the degree of back corona was not aggravated after 10 minutes of operation, thus the rates of change of electric current and collection efficiency slowed down. This indicates that as back corona occurred, more negative ions were generated by the power supply to overcome the reduction of net space charge density. As a result, the total current passed through the dust layer increased. But the phenomenon of increasing current slowed down as the ratio of positive ions to negative ions reached a stable value.

Constant applied current

Variations in the output voltages under constant applied currents for the case of without moisture conditioning are shown in Fig. 4a. One can see that the voltages dropped suddenly during tests. For an applied current of 0.6 mA, the output voltage was decreased from 42.5 kV to less than 25 kV. Hence the power consumption under a constant applied current was different from that under a constant applied voltage. The power consumption under constant applied current was reduced due to the back corona effect.

The experimental results of overall mass collection efficiency under constant current conditions are shown in Fig. 4b as a function of operation time. It is seen that the mass collection efficiencies dropped with an increase in the operation time. However, the variation of mass collection efficiencies did not show a clear trend for different applied currents. It was independent of the applied current. That is, although the lowest applied current of 0.12 mA during tests gave the smallest output voltage, its corresponding mass collection efficiency was not necessarily the lowest. One reason for that is the back corona only occurred partially and unstably on the collection plates. It was observed that only slight and unstable glints occurred at the central part of collection plates during the tests. The number of porous holes on the dust layer under the constant applied current test was also less than that under the constant applied voltage test. The unstable back corona on the collection plates produced irregular electrostatic force on the particles, thereby led to irregular variation of mass efficiency with the applied current.

Voltage–current characteristics

In order to further understand the phenomena of back corona, a simple mathematic model was developed to assist in the discussion of experimental observations. A detailed description of the mathematical model can be seen in Appendix A. The model was capable of predicting the ESP performance under the stable back corona condition. Because the back corona phenomenon was quite unstable for constant applied current, the following discussion is focused only on results obtained under constant applied voltage.

Figure 5 shows the experimental data as well as the theoretical simulation of voltage–current characteristics under constant voltage operations. The voltage–current characteristics were obtained after the observation of stable operation currents. For the case of normal condition, the voltage–current curves were the same for clean plate and dusty plate at voltages less than 33 kV. And the predicted results agreed well with the experimental measurements. The major difference between the dusty plate and the clean plate under normal conditions was the sparkover voltage. The sparkover voltage for the clean plate

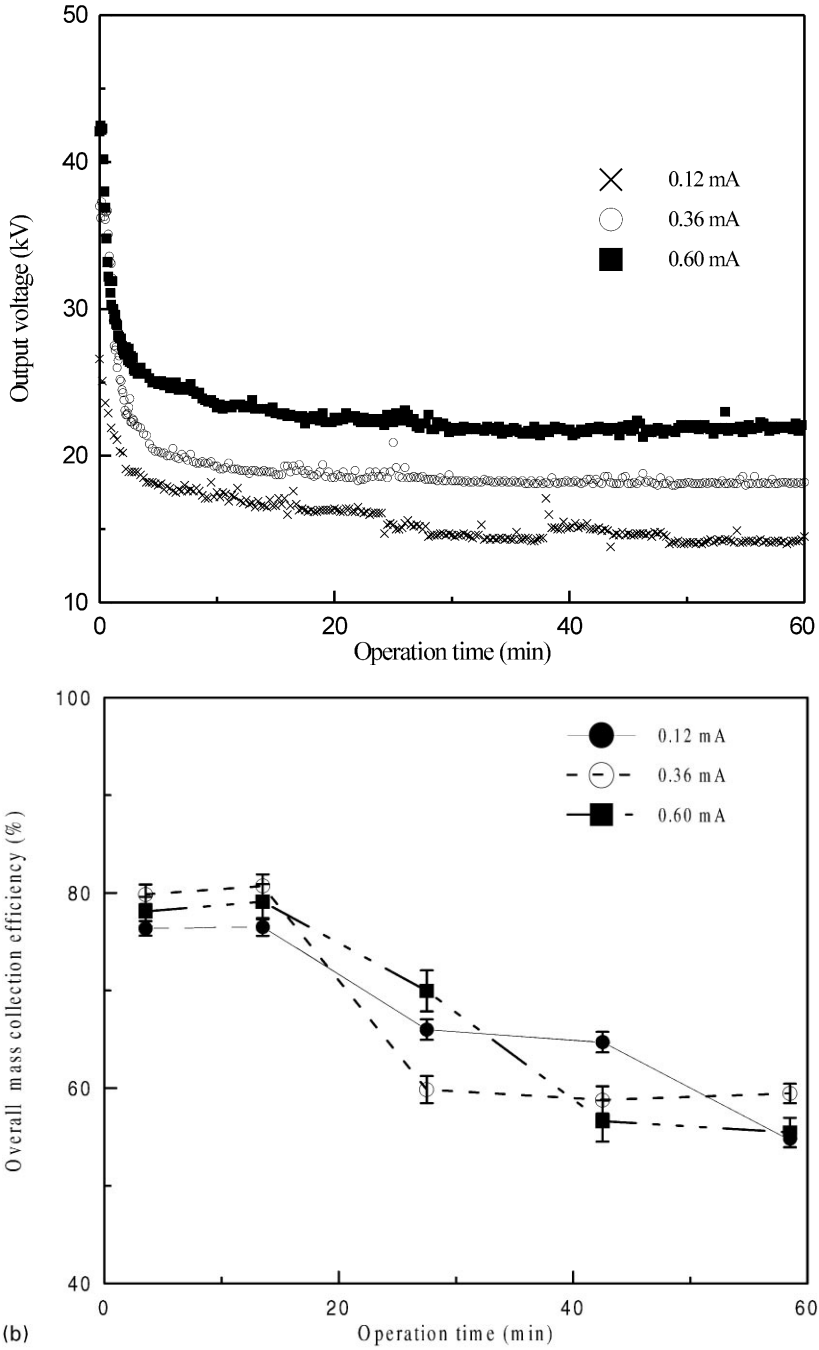

Fig. 4. Experimental results on the variation of (a) ESP output voltage with operation time under the constant applied current method without moisture conditioning and (b) overall mass collection efficiency with operation time under the constant applied current method without moisture conditioning.

operation was 48 kV, while with dust deposited on the collection plates the current suddenly increased at above 35 kV and sparks occurred.

On the other hand, the voltage–current curve under the back corona condition rose with a very fast rate. For a voltage of around 25 kV the current increased so sharply that the voltage–current curve was almost vertical. The spark occurred at a voltage of 27 kV. The spark voltage was less than that under normal conditions. An adjustable parameter, S, was used in the simulation of voltage–current characteristics of an ESP under the back corona

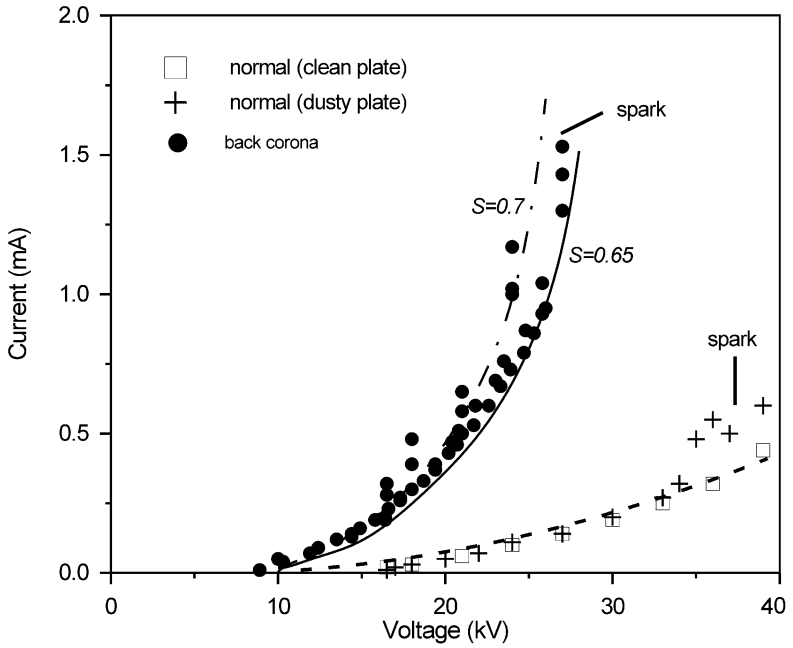

Fig. 5. Experimental and theoretical results on the voltage–current characteristic curve of the ESP. The symbols are experimental observations and lines are theoretical results.

condition. It was defined as the ratio of the space charge density of back ions to the space charge density of corona ions on the surface of the collection plate (Hoburg, 1982). Therefore, the value of S reflected the degree of back corona. The total current was increased with an increase in the value of S at a constant voltage. As the value of S was around 0.65–0.7, the theoretical voltage–current characteristic of the system under back corona agreed well with the experimental observations.

Predicting the ESP collection efficiency

The flow Reynolds number in our ESP was 988 and the flow velocity was $0.2\,\mathrm{m\,s^{-1}}$ during our experimental test. The flow pattern seems to be laminar at a first glance. In order to discuss the effects of flow mixing and the possible ion wind occurring in our experiment, a simple particle trajectory model was employed which could simulate the particle path in a non-lateral mixing flow without the presence of an ion wind. The particle trajectories for particle-sizes of 0.1–1.6 μm are show in Fig. 6. The results of the particle trajectory model indicated that particles of larger than 0.1 μm diameter would be collected by the ESP. That is, the predicted overall collection efficiency was 100% for our experimental particles under a non-lateral mixing flow condition. However, the actual measured efficiencies were around 90% under normal operation. The 10% overestimation of the collection efficiency may be due to the ion wind effect occurring during the experimental test.

Liang and Lin (1994) developed a theoretical model to investigate the effect of ion wind. They showed that at a cross flow velocity of 0.2 (the cross flow velocity was defined as u_F/u_e, where u_F and u_e were flow velocity and characteristic velocity of ionic wind, respectively), the difference in the collecting efficiency for considering/neglecting the ion wind effect is the largest. They can lead to about 12% discrepancy in the overall collection efficiency. In our experimental study the cross flow velocity was calculated to be 0.07. Therefore, a 10% difference of trajectory model prediction (which neglects the ion wind effect) and experimental data seems reasonable.

The effect of ion wind has also been conducted experimentally by Leonard *et al.* (1983). They showed that the turbulent intensity increases as the dimensionless number $I_i/L_w b\rho_F u_F^2$

increases. The dimensionless number $I_i/L_w b\rho_F u_F^2$ is a measure of the ratio of the corona-discharge-induce body force to the inertial force on the gas (where I_i/L_w is the discharge current per unit length of discharge wire, b is the ion mobility, ρ_F is the gas density and u_F is the mean gas velocity at the inlet to the precipitator). From their experimental observation, the flow mixing is appreciably increased with decreasing values of mean gas velocity due to the ion wind effect. For dimensionless number $I_i/L_w b\rho_F u_F^2 > 0.5$, the level of turbulent intensity in the core of the flow is increased in excess of the background turbulence level.

The dimensionless number in our experimental study was over 100 for normal condition. The turbulent intensity was much larger for back corona operation. Therefore although the

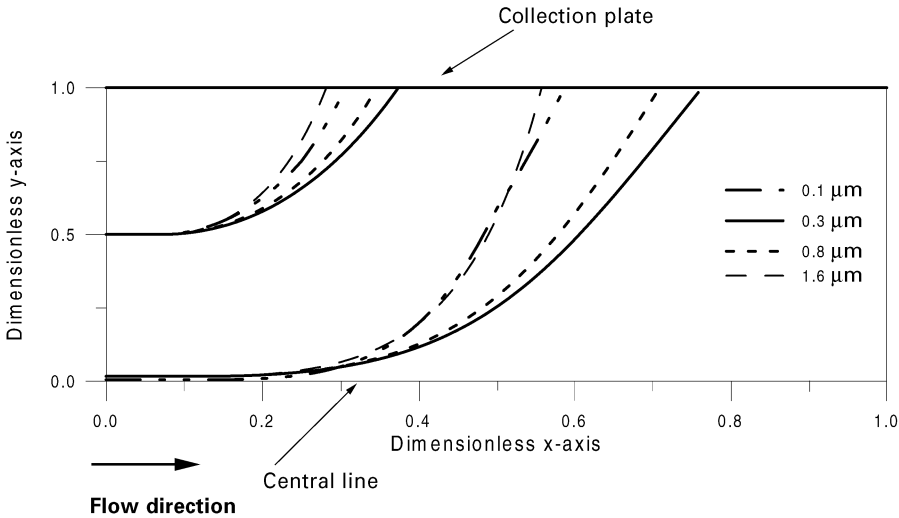

Fig. 6. Particle trajectories at 27 kV under normal operation.

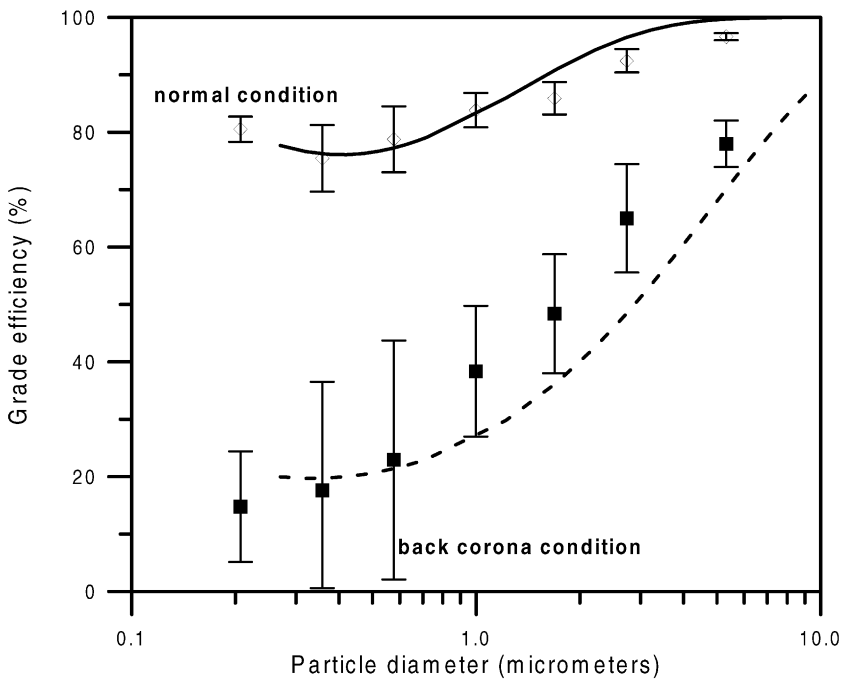

Fig. 7. The grade efficiencies of a wire-plate ESP under a constant applied voltage of 27 kV for both normal and back corona conditions. The symbols are experimental observations and lines are theoretical results from the lateral mixing model.

ion wind effect was appreciable in our experimental tests, it produced turbulence and provided well mixing of the flow, especially under back corona. Hence, the use of the Deutsch equation where lateral mixing was assumed is a reasonable assumption. It was used to predict the ESP collection efficiency under both normal and back corona conditions in the following discussion.

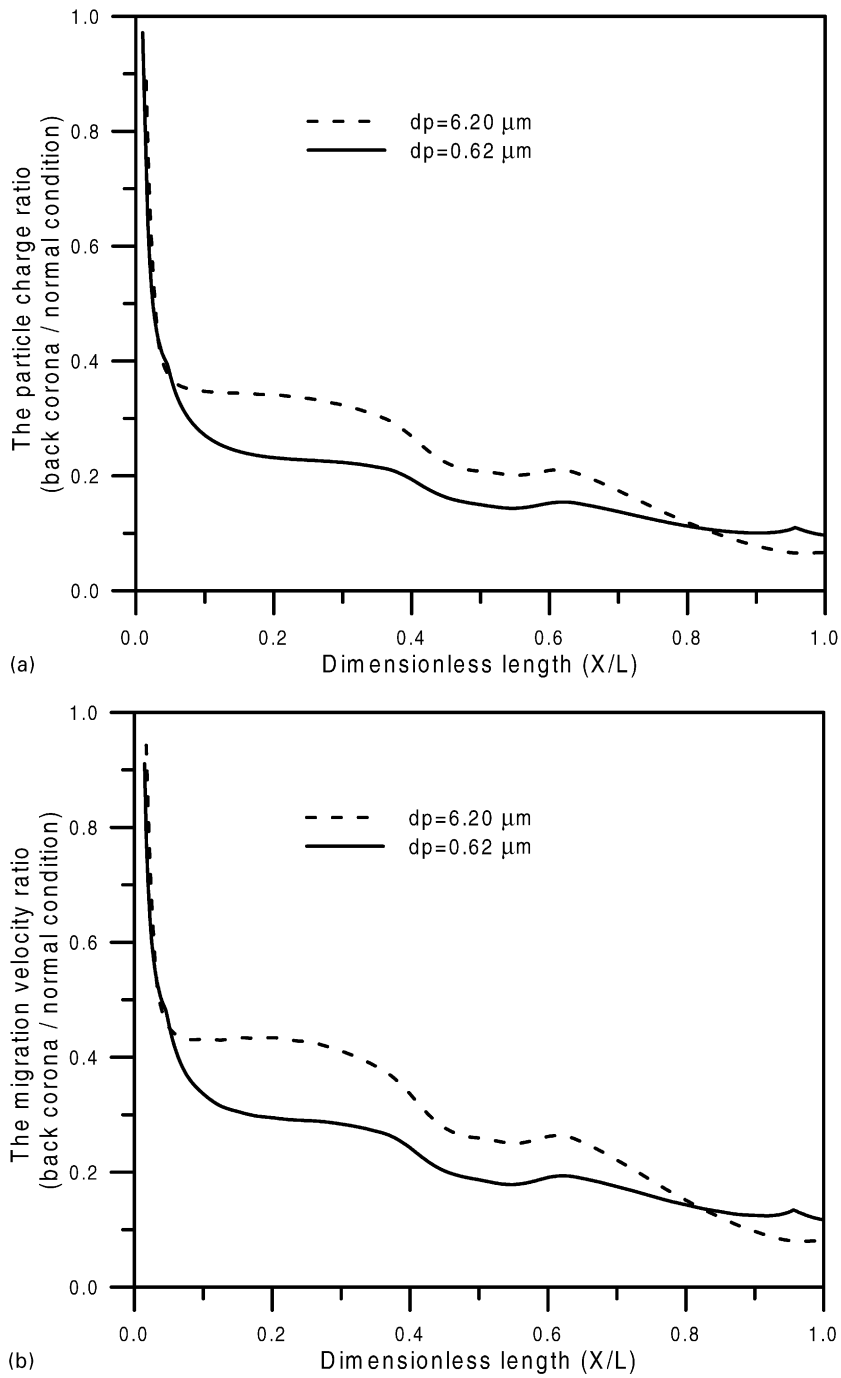

Fig. 8. Lateral mixing model results on the decreasing ratio of (a) particle charge from normal to back corona conditions as a function of ESP dimensionless length. The operation voltage was 27 kV and the degree of back corona (S) was 0.65 and (b) particle migration velocity from normal to back corona conditions as a function of ESP dimensionless length. The operation voltage was 27 kV and the degree of back corona (S) was 0.65.

Figure 7 shows the experimental results of particle grade efficiency under a constant applied voltage of 27 kV. The oscillation of current and small break downs under the back corona condition caused large deviations in the grade efficiency of repeated experiments. As can be seen from the experimental results, the back corona has a larger effect on particle sizes of less than around 1.0 μm. For example, the grade efficiency of 0.21 μm particles was reduced by over 60% due to back corona. The model results are also shown in Fig. 7. The adjustable parameter (S) was 0.65 for back corona condition. As can be seen, the theoretical results agreed well with the experimental measurements under both normal and back corona conditions, the minimum grade efficiency occurred at around 0.3 μm of the particle diameter.

The larger reduction in efficiency with smaller particles in the presence of back corona may be because the charge as well as migration velocity of smaller particles are reduced more significantly by back ions than those of larger particles. These have been demonstrated by Figs 8a and b. As can be seen in Fig. 8a, the decreasing ratios of charge of a 0.62 μm particle from normal to back corona conditions were smaller than those of a 6.2 μm diameter particle during the dimensionless length of 0.1–0.8. The significant reduction in particle charge of submicron particles from normal to back corona conditions resulted in a significant reduction of their migration velocity as shown in Fig. 8b.

After validation of the lateral mixing model under normal and stable back corona conditions, it was used to evaluate the back corona effect on the grade efficiency of particles. The parameter values used in the simulation are shown in Table 1. A full-scale ESP was assumed in the model simulation. Figure 9 shows model results on the decreasing ratios of

Table 1. Parameter values used in the simulation of the back corona effect

Gas velocity	1 m s^{-1}	Diameter of wire	0.2 mm
Temperature	130°C	Plate length	9.6 m
Wire-to-wire spacing	300 mm	Wire-to-plate spacing	140 mm

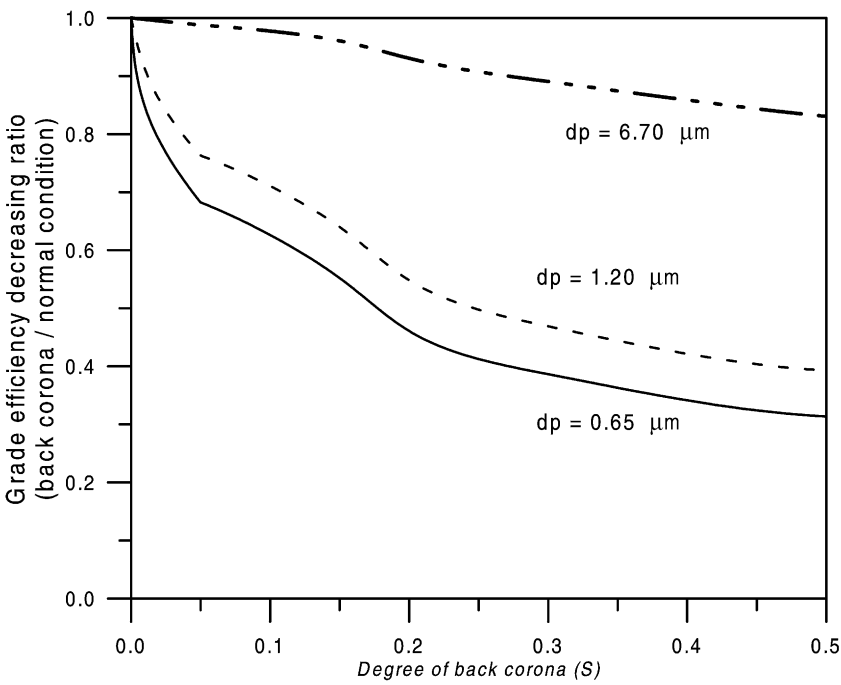

Fig. 9. Lateral mixing model results on the decreasing ratio of grade efficiency from normal to back corona conditions as a function of the degree of back corona (S).

grade efficiencies of 0.65, 1.2, 6.7 μm diameter particles as a function of S at an applied voltage of 56 kV. The increase of S reflects the degree of back corona and it reduces the collection efficiency of an ESP. One can see that the grade efficiency of smaller particles dropped significantly as the condition of the back corona got aggravated. The grade efficiency of 0.65 μm particles could be reduced to only 30% of its original efficiency at a back corona degree of 0.5. Since particles in the submicron (0.1–1.0 μm) region have a larger effect on the plume opacity, the increase of back corona may cause severe opacity problem besides decreasing the overall mass collection efficiency.

CONCLUSION

Information on the ESP performance under normal and back corona conditions was provided by experimental observation via a single discharge wire-plate ESP system. Under the constant voltage controlled method, the output current was suddenly increased and thereby power consumption was also increased by back corona. While under the constant current controlled method, the voltage was reduced by back corona and the power consumption was also reduced. A mathematical model was used to help in discussing the phenomena occurring under back corona. An adjustable parameter which reflects the degree of back corona was used to predict the corona current over a wide range of voltage.

The ESP performance data indicated that the flow during tests should be turbulent and well mixed due to the ion wind effect. Hence a lateral mixing model was used in the simulation. Both experimental data and the theoretical results showed that the phenomenon of back corona significantly reduced the grade efficiency of submicron particles. Since particles in the submicron range (0.1–1.0 μm) are more sensible to light scattering, the back corona phenomenon may cause a severe plume opacity problem. Flue gas conditioning of water injection can effectively improve the adverse effect caused by back corona. It allows the ESP to operate under a higher effective corona power and thus a higher collection efficiency can be obtained.

Acknowledgement—Support from the National Science Council through grant No. NSC85-2211-E-009-009; NSC86-2211-E-009-002 is gratefully acknowledged.

REFERENCES

Bohm, J. (1982) *Electrostatic Precipitators*. Elsevier, Amsterdam.

Fjeld, R. A. and McFarland, A. R. (1989) Evaluation of select approximations for calculating particle charging rates in the continuum regime. *Aerosol Sci. Technol.* **10,** 535–549.

Hoburg, J. F. (1982) Charge density, electric field, and particle charging in electrostatic precipitation with back ionization. *IEEE Trans. Ind. Appl.* **IA–18,** 666–672.

Kallio, G. A. (1987) Interaction of electrostatic and fluid dynamic fields in wire-plate precipitators. Ph.D. dissertation, Department of Mechanical and Materials Engineering, Washington State University.

Kwetkus, B. A. (1997) Particle precharging and fabric filtration experimental results of a corona precharger. *J. Electrostat.* **40,** 657–662.

Lawless, P. A. and Altman, R. F. (1994) ESPM: an advanced electrostatic precipitator model. *IAS Annual Meeting, IEEE Industry Applications Society*, 1519–1526.

Lawless, P. A. and Sparks, L. E. (1980) A mathematical model for calculating effects of back corona in wire-duct electrostatic precipitators. *J. Appl. Phys.* **51,** 242–256.

Leonard, G. L., Michner, M. and Self S. A. (1983) An experimental study of the electrohydrodynamic flow in electrostatic precipitators. *J. Fluid Mech.* **127,** 123–140.

Liang, W.-J. and Lin, T. H. (1994) The characteristics of ionic wind and its effect on electrostatic precipitators. *Aerosol Sci. Technol.* **20,** 330–344.

Licht, W. (1988) Air pollution control engineering: basic calculations for particulate collection, 2nd ed., p. 107. Marcel Dekker, New York.

Masuda, S. and Nonogaki, Y. (1986) Bipolar structure of a back-discharge field in an electrostatic precipitator. *IEEE Trans. Ind. Appl.* **IA-22,** 602–609.

McDonald, J. R., Smith, W. B., Spencer III, H. W. and Sparks, L. E. (1977) A mathematical model for calculating electrical conditions in wire-duct electrostatic precipitation devices. *J. Appl. Phys.* **48,** 2231–2242.

McLean, K. J. (1988) Electrostatic precipitators. *IEE Proc.* **135,** 347–361.

Patel, S. N., Rahmolow, T. D., Kjendal, R. A. and Meehan, J. J. (1985) The effect of back corona in a laboratory scale electrostatic precipitator. *IEEE Trans. Ind. Appl.* **IA-21,** 935–938.

Turner, J. H., Lawless, P. A., Yamamoto, T., Coy, D. W., Greiner, G. P., McKenna, J. D. and Vatavuk, W. M. (1988) Sizing and costing of electrostatic precipitators. Part I. Sizing consideration. *J. Air Pollut. Control Assoc.* **38,** 458–471.
Vincent, J. H. (1989) *Aerosol Sampling Science and Practice*, p. 221. Wiley, New York.
White, H. J. (1974) Resistivity problems in electrostatic precipitation. *J. Air Pollut. Control Assoc.* **24,** 314–338.
Yamamoto, T. and Velkoff, H. R. (1981) Electrohydrodynamics in an electrostatic precipitator. *J. Fluid Mech.* **108,** 1–18.

APPENDIX A: DESCRIPTION OF MATHEMATICAL MODEL

Collection efficiency

This model assumed that particles are well mixed by lateral turbulence in the gas stream (Licht, 1988). As shown in Fig. A1, the charging cell is divided into many small size steps. The governing equation is given by

$$\eta_{i,j} = -\frac{\mathrm{d}n_{i,j}}{n_{i,j}} = \omega_{i,j}\frac{\mathrm{d}t}{W/2} = \omega_{i,j}\frac{A_{\mathrm{cj}}}{Q}, \tag{A1}$$

where $\eta_{i,j}$ is the collection fraction for the ith particle size in the jth increment length of an ESP, A_{c_j} is the collection plate area in the jth length increment, and $\omega_{i,j}$ is the migration velocity of the ith particle in the jth length increment. The overall grade efficiency is obtained from

$$\begin{aligned}\eta_{d_{\mathrm{p}}} &= 1-(1-\eta_{i,1})(1-\eta_{i,2})\ldots(1-\eta_{i,j-1})(1-\eta_{i,j})\\ &= 1-\prod_{j=1}(1-\eta_{i,j})\end{aligned} \tag{A2}$$

The effective migration velocity ($\omega_{i,j}$) of a particle of diameter d_{p} is

$$\omega_{i,j} = q_{i,j}E_{\mathrm{p}_j}C/3\pi\mu d_{\mathrm{p}} \tag{A3}$$

where $q_{i,j}$ is the charge on the particle in each j step, C is the Cunningham correction factor; μ is the gas viscosity; and E_{pj} is the field strength on the plate.

The collecting field strength ($E_{\mathrm{p}j}$) and charge of the particle ($q_{i,j}$) are determined by electrical state of the ESPs and charging theory, respectively, as described in the following.

Electric state

The electric state of an ESP generally includes items such as the current–voltage relationship, electric field and the current density pattern in the inter-electrode. They influence the electric field and particle charging rate. Main equations that govern the electric conditions in an ESP are the Poisson's equation and current continuity equation (McLean, 1988).

Normal condition. Under normal unipolar of negative ion conditions, the governing equations are

$$\nabla^2 V = -\frac{\rho_-}{\varepsilon_0}, \tag{A4}$$

$$E = -\nabla V, \tag{A5}$$

$$\nabla \cdot J = 0, \tag{A6}$$

$$J = \rho_- b^- E, \tag{A7}$$

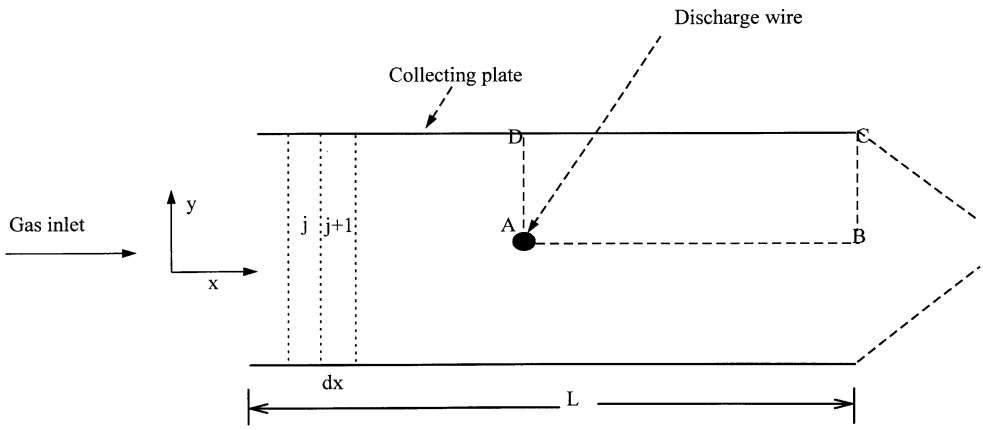

Fig. A1. Schematic diagram of a wire-plate discharge cell showing the coordinate of numerical calculation.

where V is the voltage, ρ_- is the space charge density associated with ions generated by the central electrode, ε_0 is the permittivity in free space, E is the electric field, J is the current density, and b^- is the ion mobility. McDonald *et al.* (1977) employed a finite difference method to solve the two-dimensional form of equations (A4)–(A7). In this study, similar approach is made to determine the electric state in the charging unit.

Back corona condition. For back corona condition, bipolar ions co-exist in the duct of an ESP. Assuming that the ion recombination can be neglected (Lawless and Sparks 1980), equation (A4) and equation (A7) become

$$\nabla^2 V = -\frac{(\rho_- - \rho_+)}{\varepsilon_0}, \tag{A8}$$

$$J = (\rho_- b^- + \rho_+ b^+)E, \tag{A9}$$

where ρ_- is the space charge density associated with ions generated by the collection electrodes. The space-charge density of positive ions are determined by the ratio of back ionization to corona ion flux through the surface of collection plates. The adjustable parameter, S, is used to reflect the degree of back corona. The factor is defined as (Hoburg, 1982)

$$S = \rho_{+s}/\rho_{-s}, \tag{A10}$$

where ρ_{+s} is the space charge density of back ions on the surface of the collection plates; and ρ_{-s} is the space charge density of corona ions on the surface of the collection plates.

Boundary conditions and calculation procedure

Normal condition. The boundary conditions for V in the computational domain shown in Fig. A1 are written as

$$V = V_a \quad \text{at the wire,} \tag{A11}$$

$$\rho = \rho_i \quad \text{at the wire,} \tag{A12}$$

$$V = 0 \quad \text{along the collecting plate,} \tag{A13}$$

$$\partial V/\partial y = 0 \quad \text{along the line AB,} \tag{A14}$$

$$\partial V/\partial x = 0 \quad \text{along the line AD and BC,} \tag{A15}$$

where V_a is the applied voltage at wire and ρ_i is the corona space-charge density at wire. The inner areas before the entrance and after the exit of ESP were isolated with silicon. The distance between the right-side boundary and the wire can be assumed to be sufficiently large compared with the distance between the wire and the collection plate so that the symmetric boundary condition can be used as an exit condition (Yamamoto and Velkoff, 1981).

The calculation starts by solving the space-charge-free form of equation (A4). Then the entire charge density distribution is calculated from the current continuity equation (A6). The total current relation with charge density at the wire is given by

$$\rho_i = \frac{I_i/L_w}{2\pi b_- r_i E_i}, \tag{A16}$$

where r_i is the radius of the ionized sheath, E_i is the electric field strength at the boundary of the ionized sheath, L_w is the length of the corona wire. The product $r_i E_i$ in equation (A16) can be determined by a common simplifying assumption (McDonald *et al.*, 1977)

$$r_i E_i = a_c E_c \tag{A17}$$

and E_c is electric field strength at the surface of the corona wire,

$$E_c = 3 \times 10^6 (\delta + 0.03(\delta/a_c)^{1/2}), \tag{A18}$$

where δ is the relative density of air; and a_c is the radius of the corona wire. Calculations of V and ρ_- are repeated at every grid point, and the potential at the wire is adjusted to meet convergence criteria. The convergence criteria are that the potential value at each grid point should be within 0.1 V of its previous value, and the total current density at the plate equals the given value

$$\left| \frac{(J_p)_{given} - (J_p)_{calculated}}{(J_p)_{given}} \right| \leqslant 10^{-4}, \tag{A19}$$

where

$$(J_p)_{given} = I_i/2LL_w \tag{A20}$$

and $(J_p)_{calculated}$ is given by equation (A7).

Back corona condition. The boundary conditions of back corona are the same as those under normal conditions. The major difference between back corona and normal conditions is that positive ions are generated from the collection plates under back corona. The boundary conditions of space charge of positive ions on the plate is given by equation (A10). The calculation procedure for the bipolar field is similar to the unipolar field. The value of S is set to zero initially, the value of ρ_{-s} is obtained under normal conditions. Then the value of ρ_{+s} is given by equation (A10) and the back ion charge density distribution is calculated from the current continuity equation (A6). The procedure is repeated for calculating values of potential, negative charge density and positive charge

density in the grid by adjusting the voltage at the wire to meet the convergence criteria. The value of S in equation (A10) is determined by fitting with the experimental voltage-current curve.

The grid number in the numerical calculation is 21×21 for calculation. The ion mobility for positive and negative ions were determined by equations (A21) and (A22) (Kallio, 1987).

$$b^+ = 1.36 \times 10^{-4} \left(\frac{T}{273}\right)\left(\frac{760}{P}\right) \quad \mathrm{m^2/V^{-1}\,s^{-1}}, \tag{A21}$$

$$b^- = 1.768 \times 10^{-4} \left(\frac{T}{273}\right)^{1.51}\left(\frac{760}{P}\right) \quad \mathrm{m^2\,V^{-1}\,s^{-1}}. \tag{A22}$$

The positive ion mobility at 130°C and 760 mm H_2O is $2.0 \times 10^{-4}\,\mathrm{m^2/V^{-1}\,s^{-1}}$, and for negative ions it is $3.2 \times 10^{-4}\mathrm{m^2/V^{-1}\,s^{-1}}$.

Charging theory

Particles in a corona field are charged simultaneously by both field and diffusion charge. The approximate charging equations (Lawless and Altman, 1994) which combine the two charging rates are used for calculating the charge of particles

For $\upsilon < 3\psi$:

$$\frac{\mathrm{d}\upsilon}{\mathrm{d}\tau} = \frac{3\psi}{4}\left(1 - \frac{\upsilon}{3\psi}\right)^2 + f(\psi). \tag{A23}$$

For $\upsilon \geqslant 3\psi$:

$$\frac{\mathrm{d}\upsilon}{\mathrm{d}\tau} = f(\psi)\frac{(\upsilon - 3\psi)}{\exp(\upsilon - 3\psi) - 1} \tag{A24}$$

and

$$\upsilon = \frac{q q_\mathrm{e}}{2\pi\varepsilon_0 d_\mathrm{p} kT}, \tag{A25}$$

$$\psi = \frac{q_\mathrm{e} d_\mathrm{p} E}{2kT}, \tag{A26}$$

$$\tau = \frac{\rho_-}{\varepsilon_0} b^- t, \tag{A27}$$

$$f(\psi) = \sin\left(\arctan\left(\frac{1.13}{\psi^{1/2}}\right)\right), \tag{A28}$$

where the value of 3ψ is commonly called the saturation charge of the field charge, q_e is the unit electron charge, k is the Boltzmann's constant, T is the absolute temperature, and t is the actual residence time.

For the back corona condition where opposite currents of positive and negative ions present in the duct of an ESP, the charging rate of particles is described as (Fjeld and McFarland, 1989)

$$\frac{\mathrm{d}\upsilon}{\mathrm{d}\tau} = \left(\frac{\mathrm{d}\upsilon}{\mathrm{d}\tau}\right)^+ - \frac{1}{\gamma}\left(\frac{\mathrm{d}\upsilon}{\mathrm{d}\tau}\right)^-, \tag{A29}$$

where

$$\gamma = \frac{b^+\rho_+}{b^-\rho_-}. \tag{A30}$$

To calculate electric states at different locations, the above charging equations (A23), (A24), and (A29) must be rewritten as

$$\frac{\mathrm{d}q}{\mathrm{d}t} = (\text{Equation (A23), (A24) or (A29)}) \times \left(\frac{\rho_-}{\varepsilon_0} b^-\right) \Big/ \left(\frac{q_\mathrm{e}}{2\pi\varepsilon_0 kT}\right), \tag{A31}$$

The electric field (E) and space charge density (ρ_-, ρ_+) are changed as the particle path changes. Average values of space charge and field strength in each j length are used for calculating particle charge equation (A31). The fourth-order adaptive-step-size Runge–Kutta numerical method is employed and the length of each j step is 10^{-6} m.

The distributions of average space-charge density and electric field are shown in Figs A2 and A3, respectively, at an applied voltage of 27 kV. The origin and the end point of dimensionless length represent the inlet and outlet of the ESP cell. For the condition of stable back corona, the corona charge (negative ions) density is larger than that under normal conditions due to the existence of positive ions. A higher electric field strength on the collection plate is also observed under back corona.

Particle trajectory method

When the calculation is based on the assumption that particles are not laterally mixed, the two dimensional particle trajectory model is used. The equation of particle motion for the discharge cell is written as

$$\frac{\mathrm{d}\boldsymbol{u}_\mathrm{p}}{\mathrm{d}t} = \frac{3}{4d_\mathrm{p}}\frac{\rho_\mathrm{F}}{\rho_\mathrm{p}} C_\mathrm{D} |\boldsymbol{u}_\mathrm{F} - \boldsymbol{u}_\mathrm{p}| (\boldsymbol{u}_\mathrm{F} - \boldsymbol{u}_\mathrm{p}) + \frac{q}{m_\mathrm{p}}\boldsymbol{E} \tag{A32}$$

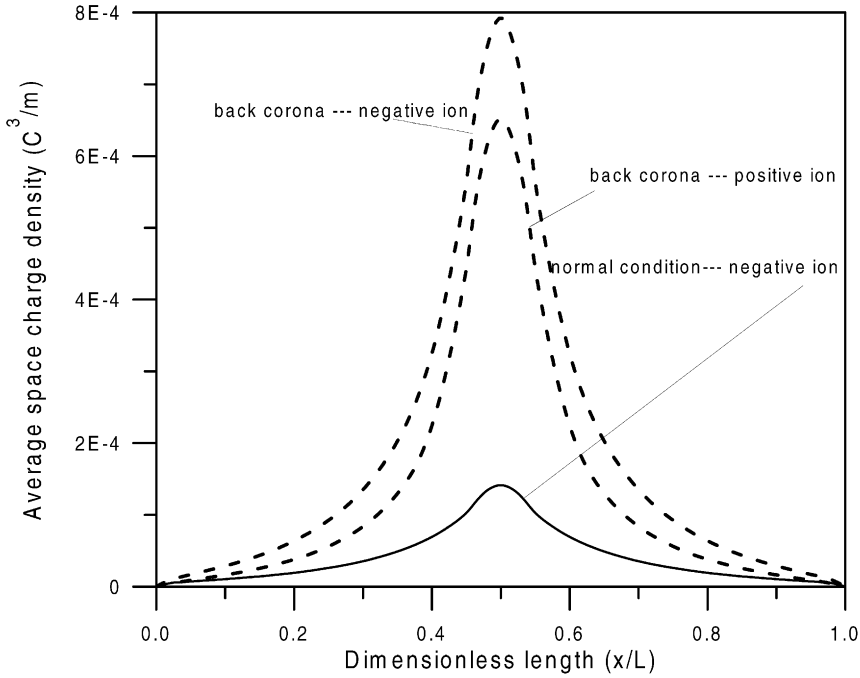

Fig. A2. Calculated distributions of the average space charge in the charging cell under normal conditions and back corona ($V = 27$ kV).

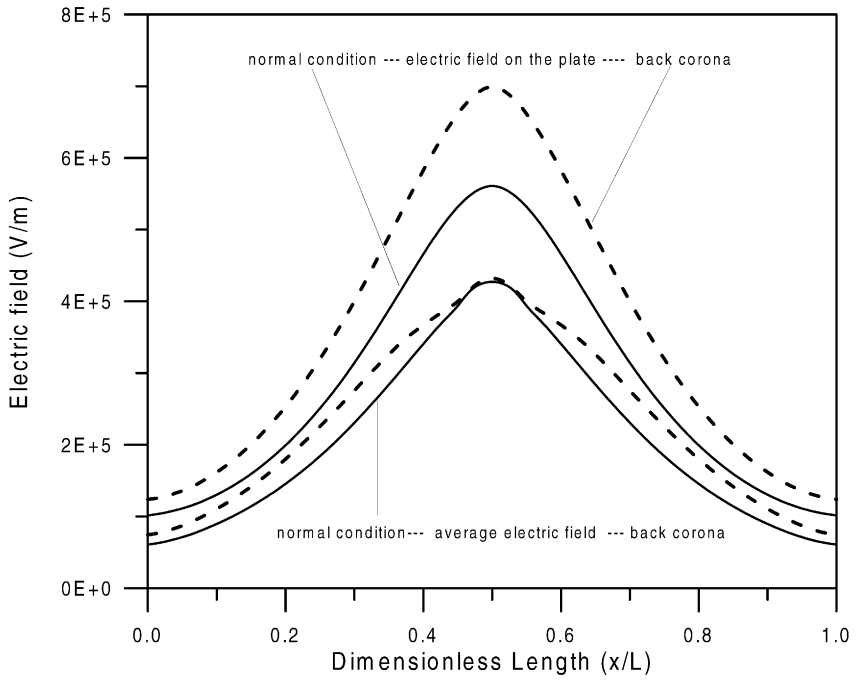

Fig. A3. Calculated distributions of electric field strength in the charging cell under normal condition and back corona ($V = 27$ kV).

where u_p is the particle velocity, u_F is the average gas velocity, ρ_p is the particle density, ρ_F is the gas density, m_p is the mass of particle, and C_D is the drag coefficient. The electric state and space-charge density used in the calculation of the particle trajectory method are the same as those previously described. Values of the electric field and space-charge density between two connected grids are obtained through polynomial regression.